Cascaded modulator-chicane modules for optical manipulation of relativistic electron beams

Erik Hemsing and Dao Xiang
SLAC National Accelerator Laboratory, Menlo Park, California 94025, USA
(Received 24 October 2012; published 28 January 2013)

A sequential arrangement of three pairs of modulators and dispersive sections that performs precise manipulation of a relativistic electron beam's longitudinal phase space is described. We show that using only a single laser wavelength, this scheme acts as a waveform synthesizer through linearization of local regions of phase space to generate sawtooth, triangular, and square wave-type distributions. It also acts as an optical analog of an rf function generator to generate intense coherent radiation that has periodic triangle and square field profiles at the optical wavelength. The same setup can also be used to improve the high-harmonic bunching factors in echo-enabled harmonic generation schemes up to 25% and to produce a bunching factor above 90% at the laser fundamental wavelength for high-efficiency capture in inverse free electron laser acceleration applications.

DOI: 10.1103/PhysRevSTAB.16.010706 PACS numbers: 41.75.Ht, 41.60.Cr, 42.65.Ky, 29.27.−a

I. INTRODUCTION

Recent advances in the generation and control of high-brightness electron beams (e-beams) have lead to a new class of intense accelerator-based light sources capable of examining matter at Angstrom wavelengths and femtosecond time scales [1]. With these advances has come tremendous progress in the techniques of optical-scale manipulation of the e-beam phase space. Born of demands to improve the harmonic content, coherence, or beam quality of the coherent radiation from these facilities, such techniques also provide new opportunities to produce e-beams that themselves may be of use for probing nature at the smallest scales [2,3].

One of the more robust ways to precisely manipulate the e-beam is through the interaction of the beam with a laser inside a magnetic undulator. In the laser modulator (M), the laser exchanges energy with the e-beam, generating a sinusoidal energy modulation in the e-beam longitudinal phase space. This stage is often followed by a dispersive magnetic chicane (C) that introduces a momentum compaction factor to convert the energy modulation into a density modulation. Several distinct combinations of this arrangement are currently used to tailor the e-beam energy and density distribution. High harmonics of the laser frequency can be generated in the e-beam density distribution, making this approach powerful for harmonic radiation schemes such as high-gain harmonic generation (HGHG) [4–6]. Higher harmonics can be obtained by cascading HGHG with radiators [7], or by using two pairs of modulators (M-C-M-C) as in echo-enabled harmonic generation (EEHG) [8–11]. Strong density modulations imposed at wavelengths much longer than the radiation wavelength produce regions of high-current that can enhance the output of self-amplified spontaneous emission (SASE) in free-electron lasers (FELs) [12], or be used for the production of a train of phase-locked pulses in x-ray FELs [13,14]. Increasing the density modulation—or bunching factor—also leads to increased efficiency in inverse FEL (IFEL) accelerator applications [15,16], where an M-C prebuncher is used as an injector to increase the number of particles at the optimal phase of the high-power drive laser field, which accelerates the beam [17]. Laser modulators using higher-order transverse interactions have also been proposed for subfemtosecond longitudinal profile diagnostics [18], and to perform mode–up-conversion of the laser profile for the production of light with orbital angular momentum [19–21].

In this paper we examine an arrangement of three pairs of laser modulators and chicanes (M-C-M-C-M-C) to perform precise manipulation of the electron beam for several purposes, namely, (1) for the synthesis of optical-scale waveforms in the phase space and in the emitted coherent radiation, (2) as a method to enhance the high-harmonic microbunching in EEHG, and (3) for the production of a nearly ideally prebunched beam. We focus specifically on a layout in which the same wavelength is used in each section. Shown in Fig. 1, this design enables the use of a single laser and thus eases demands on the precision timing control of the e-beam and laser between sections. We show that successive single-frequency modulations interspersed by dispersive elements can be used to synthesize a train of periodic sawtooth, triangle, and square waveforms in the longitudinal phase-space distribution. This results in an e-beam analog of an rf function generator, but at the optical scale. Alternatively, the scheme can also be used to generate periodic square and triangle waveforms in the integrated e-beam current distribution. In a broadband radiator, the beam emits optical fields with temporal structures that replicate the current profile, therefore this technique can be

Published by the American Physical Society under the terms of the Creative Commons Attribution 3.0 License. Further distribution of this work must maintain attribution to the author(s) and the published article's title, journal citation, and DOI.

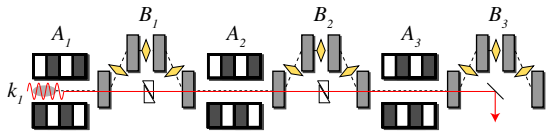

FIG. 1. Triple modulator and chicane layout. The timing of single laser in each section can be adjusted by adjustable phase delay. Variable quadrupoles between bends in the chicanes (yellow diamonds) permits reversal of the sign of the momentum compaction.

used as an optical waveform generator to produce instantaneous fields with square or triangle waveforms at the optical wavelength. Both of these techniques may have compelling applications in ultrafast science and quantum control [22,23]. We show that a linearization procedure also enables this technique to improve the harmonic bunching in EEHG applications. Finally, we also present a scenario in which the beam bunching factor at the laser frequency exceeds 90%, suggesting a way to significantly increase the capture and acceleration efficiency in modern IFEL applications [24].

We note that the versatile triple modulator/chicane scheme has been explored previously in different contexts. In [25] the setup was examined as a method to strongly upconvert the frequency of a low-power, short wavelength laser in order to seed an x-ray FEL. An alternate arrangement (M-C-M-M-C) in which the wavelength of the third modulation is large was described in [26] as a way to combine EEHG with compression from a linear chirp to produce an attosecond x-ray pulse. An extension of this was introduced in [27] for the production of a train of attosecond pulses for amplification in a mode-locked x-ray FEL. In [28], an arrangement in which the first M-C section density modulates the beam was proposed as a technique to enhance the performance of EEHG for the production of high harmonics. Thus, given the multitude of optimizations and modularity of the setup, what we present is not meant to be exhaustive, but merely to outline several new additional advanced applications.

II. BEAM EVOLUTION AND BUNCHING FACTOR

Consider an e-beam with energy E_0 described by a Gaussian distribution function $f(p_0) = (2\pi)^{-1/2} e^{-p_0^2/2}$, where $p_0 = (E - E_0)/\sigma_E$ is the scaled energy of an electron with energy E and σ_E is the beam energy spread. The energy modulation and longitudinal coordinate transformations performed by N successive modulator and dispersion pairs is given generally by

$$\begin{aligned} p_N &= p_{N-1} + A_N \sin(k_N z_{N-1} + \phi_N), \\ z_N &= z_{N-1} + B_N p_N / k_1, \end{aligned} \tag{1}$$

where $p_N = (E_N - E_0)/\sigma_E$ is the scaled energy after the Nth modulation at the frequency k_N, $A_N = \Delta E_N/\sigma_E$ is the modulation amplitude, ϕ_N is the laser phase, and z_N is the electron's longitudinal coordinate. The longitudinal dispersion is $B_N = R_{56}^{(N)} k_1 \sigma_E / E_0$, where $R_{56}^{(N)}$ is the momentum compaction. The longitudinal complex-valued bunching factor at the frequency k can be calculated from

$$b(k) = \left\langle \int e^{-ikz_N} f_f(z_N, p_N) dp_N \right\rangle, \tag{2}$$

where $f_f(z_N, p_N)$ is the final e-beam distribution, and brackets denote averaging over the final coordinates, $\langle \cdots \rangle = \lim_{L\to\infty} \frac{1}{2L} \int_{-L}^{L} \langle \cdots \rangle dz_N$.

We consider a series of three modulator/dispersive sections ($N = 3$). The bunching factor for a beam much longer than the modulation wavelengths has sharp peaks at the frequencies

$$k \equiv ak_1 = (n + mK_2 + lK_3)k_1, \tag{3}$$

where $K_2 = k_2/k_1$ and $K_3 = k_3/k_1$ and n, m, and l are integers. At this frequency the bunching is given by

$$b(ak_1) = \sum_{n,m,l=-\infty}^{\infty} b_{n,m,l} \delta_{a,n+mK_2+lK_3}. \tag{4}$$

A full expression for the bunching factor $b_{n,m,l}$ is given in the Appendix, Eq. (A2). Concentrating on identical wavelengths between sections, we set $K_2 = K_3 = 1$. The harmonic number is therefore an integer and we can make the replacement $l = a - n - m$ to obtain

$$b(ak_1) = \sum_{n,m=-\infty}^{\infty} b_{n,m}, \tag{5}$$

where

$$\begin{aligned} b_{n,m} = {} & e^{-\xi_{n,m}^2/2 + im(\phi_2 - \phi_3) + i(a-n)\phi_3} \\ & \times J_n(-A_1 \xi_{n,m}) J_m[-A_2(n+m)B_2 - aA_2B_3] \\ & \times J_{a-n-m}[-aA_3B_3] \end{aligned} \tag{6}$$

and

$$\xi_{n,m} = n(B_1 + B_2) + mB_2 + aB_3. \tag{7}$$

We have set the relative phase factor $\phi_1 = 0$ for convenience.

III. PHASE-SPACE WAVEFORM SYNTHESIZER

A. Synthesis with laser harmonics

Simple periodic sawtooth, triangle, and square waveforms are mathematically described by an infinite sum of sine waves and their harmonics. An ideal sawtooth wave of amplitude A and periodicity $\lambda = 2\pi/k$ is obtained with the infinite Fourier series of all harmonics,

$$x_{\text{saw}}(z) = \frac{2A}{\pi} \sum_{h=1}^{\infty} (-1)^h \frac{\sin(hkz)}{h}. \tag{8}$$

A square wave is similarly expressed by a sum of only odd harmonics,

$$x_{\mathrm{squ}}(z) = \frac{4A}{\pi} \sum_{h=1}^{\infty} \frac{\sin[(2h-1)kz]}{(2h-1)}, \tag{9}$$

as is a triangular wave, albeit with different harmonic amplitudes and phases:

$$x_{\mathrm{tri}}(z) = \frac{8A}{\pi^2} \sum_{h=1}^{\infty} (-1)^{h-1} \frac{\sin[(2h-1)kz]}{(2h-1)^2}. \tag{10}$$

Such waveforms are ubiquitous in a wide range of applications. However, the crucial feature relevant to high-brightness beams is the potential to introduce linearity in the phase space through harmonic modulation. This can lead to increases in both the obtainable bunching factor in harmonic generation schemes [29,30], and in particle capture efficiency [17].

The triple modulator/chicane setup can be used in two distinct ways to generate each of these waveform distributions. Conceptually, the most straightforward way is to modulate the beam with three harmonic wavelengths with the proper amplitudes and phases following Eqs. (8)–(10). Figure 2 shows the resulting distributions with zero dispersion between modulations. The phase space evolves into a waveform that approaches the ideal with each step, showing distinct and increasingly flatter regions of *macrolinearity*. For sawtooth and square waves, the macrolinear regions also contain a greater fraction of electrons, which makes them useful for further manipulation or radiation production downstream. Consider a dispersion section (B_3) placed after the final modulation section. Dispersion by $B_3 = \pi/2A$ of a square waveform distribution, for example, shifts the flattop regions to the same phase position. This suggests a method for creating precisely separated, quasimonoenergetic energy bands for the amplification of subfemtosecond pulse structures via the two-stream instability [31]. In a sawtooth wave, the slope of the macrolinear portion approaches $-k_1 A/\pi$, for which a dispersion of $B_3 = \pi/A_1$ leads to enhanced bunching from that of a single-frequency modulator. With three sections, analysis shows that the maximum achievable bunching at the $a = 1$ fundamental is $\sim$80% versus 58% for a single stage, which could improve IFEL performance [17]. Used as a seed for HGHG, such a distribution leads to marked improvement in the high-harmonic bunching factors which relaxes demands on the downstream radiator for the production of intense

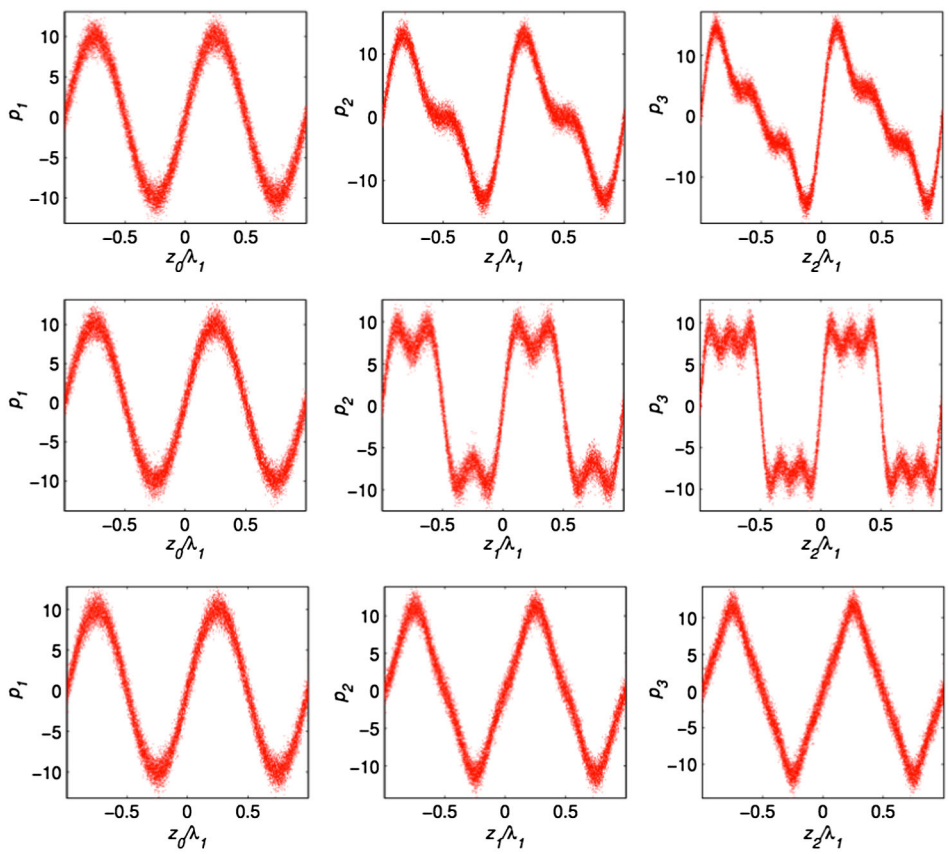

FIG. 2. Waveform generation through harmonic modulation. Different waveforms are shown in independent rows. The left column is the modulation by one laser, the middle column is with two lasers, and the right column is with three lasers. Top: Sawtooth wave generation with modulations of wavelengths λ_1, $\lambda_2 = \lambda_1/2$, and $\lambda_3 = \lambda_1/3$. Here $A_1 = 10$, $A_2 = A_1/2$, $A_3 = A_1/3$, $B_1 = B_2 = 0$, $\phi_2 = \phi_3 = 0$. Middle: Square wave generation with $\lambda_2 = \lambda_1/3$, $\lambda_3 = \lambda_1/5$, $A_1 = 10$, $A_2 = A_1/3$, $A_3 = A_1/5$, $B_1 = B_2 = 0$, $\phi_2 = \phi_3 = 0$. Bottom: Triangle wave with $\lambda_2 = \lambda_1/3$, $\lambda_3 = \lambda_1/5$, $A_1 = 10$, $A_2 = A_1/9$, $A_3 = A_1/25$, $B_1 = B_2 = 0$, $\phi_2 = \pi$, and $\phi_3 = 0$.

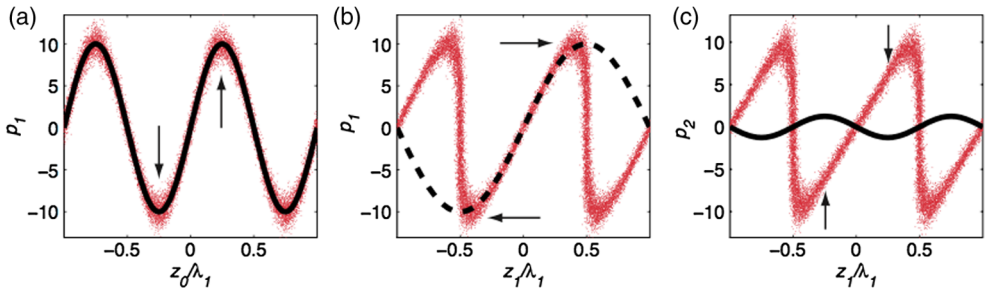

FIG. 3. Local linearization with a dispersive section between two modulations at the same wavelength, λ_1. The beam is first modulated with amplitude A_1 (a), and then longitudinally dispersed by $B_1 = 1/A_1$ (b). This distributes particles in the region $-\lambda_1/2 < z_1 < \lambda_1/2$ along a sinusoid with wavelength $2\lambda_1$ (dashed line). A subsequent smaller modulation A_2 shifted by π (solid line), removes the curvature in the decompressed region (c).

coherent light [30]. A similar benefit is obtained in EEHG seeding schemes, where the ultrahigh harmonics are enhanced by optical manipulation of the sawtooth in subsequent sections [29,30].

B. Synthesis with single laser

With dispersive sections between modulators however, there is another method by which analogous such waveforms can be generated in the longitudinal phase space. Further, by the transformative effects of dispersion, they emerge using the same wavelength laser in each modulator, which suggests an arrangement where a single laser pulse can be used in all three sections to relax synchronization constraints (discussed later). It allows the modulators to have the same tuning, with the modulation amplitudes controlled by number of periods and/or laser spot size, for example. The concept is based on piecewise manipulation of specific phase-space regions, and is shown in Fig. 3.

The technique is illustrated by examination of the local phase space at each step. The energy modulation generated by an initial sinusoidal laser field [Fig. 3(a)] creates a local chirp in the beam as a function of z_0 given by $C = dp_1/dz_0 = A_1 k_1 \cos(k_1 z_0)$. Particles near the $k_1 z_0 = 0$ zero crossing have a positive chirp ($C > 0$), whereas those near $k_1 z_0 = \pm\pi$ have a negative chirp ($C < 0$). After passage through the following dispersion section [Fig. 3(b)], the region where $C > 0$ becomes stretched, or decompressed, while the negatively chirped region is compressed. At a dispersion strength of $B_1 \simeq 1/A_1$, the negatively chirped regions at $k_1 z_0 = \pm\pi$ are fully compressed, and half of the particles are localized to this narrowed region of phase. The other half are stretched over the decompressed region extending from $-\lambda_1/2$ to $\lambda_1/2$ and form a shape that approximates a sinusoid with twice the wavelength of λ_1. We see that through dispersion, the second laser (with $k_2 = k_1$) now interacts effectively like the second harmonic frequency in this stretched region of the phase space, and can therefore be used to partially linearize [as shown in Fig. 3(c)] or otherwise manipulate the local distribution in the second modulating section. Linearization requires shifting the laser phase in the second section by $\phi_2 = \pi$ to correct the initial curvature and to leave particles in the fully compressed regions (where the electrons are piled up in z) essentially unaffected by the second modulation since they are at the zero field crossing.

The same procedure can then be performed on the electrons in the compressed region by reversing the sign of the second dispersive section, $B_2 \simeq -2B_1$, and acting on the beam with the third modulator. Again, decompression enables harmonic manipulation in this portion with the third laser with frequency $k_3 = k_1$ at $\phi_3 = \pi$ (in phase with the laser in the second modulator). By setting A_2 and A_3 to compensate for the dominant sinusoidal curvature, one can use this method to synthesize the linear regions of the triangular waveform. Shown in Fig. 4, the resulting distribution is a series of partially linearized sections with alternating signs of local chirp. Depending on the magnitude of the third chicane, the final distribution is that of a synthetic sawtooth with either left or right facing slopes, or a nearly ideal triangular waveform.

To get a feel for the required modulations and dispersions, it is useful to track the evolution of the particles at the design orbit ($p_0 = 0$) through the first three successive transformations. After the first modulator the electron energy is $p_1 = A_1 \sin(k_1 z_0)$, and after the chicane the new position is $z_1 = z_0 + B_1 p_1/k_1$. Combining these and solving for p_1 in terms of z_1, the energy after the second modulation $p_2 = p_1 + A_2 \sin(k_1 z_1 + \phi_2)$ can be expanded near $z_1 = 0$ as

$$\begin{aligned} p_2 \simeq\ & A_2 \sin\phi_2 \left(1 - \frac{(k_1 z_1)^2}{2!} + \frac{(k_1 z_1)^4}{4!} \cdots\right) \\ & + k_1 z_1 \left(\frac{A_1}{1 + A_1 B_1} + A_2 \cos\phi_2\right) \\ & - \frac{(k_1 z_1)^3}{3!} \left(\frac{A_1}{(1 + A_1 B_1)^4} + A_2 \cos\phi_2\right). \end{aligned} \tag{11}$$

Prior to the second modulation, a dispersion strength of $B_1 = 1/A_1$ (or $R_{56}^{(1)} = \lambda_1 E_0 / 2\pi \Delta E_1$) results in a linear chirp of $C = A_1 k_1/2$, confirming decompression by a factor of 2 after the chicane. The local distribution thus resembles a subharmonic $2\lambda_1$ modulation with amplitude A_1. From Eq. (11) we find that a laser phase in the second stage of

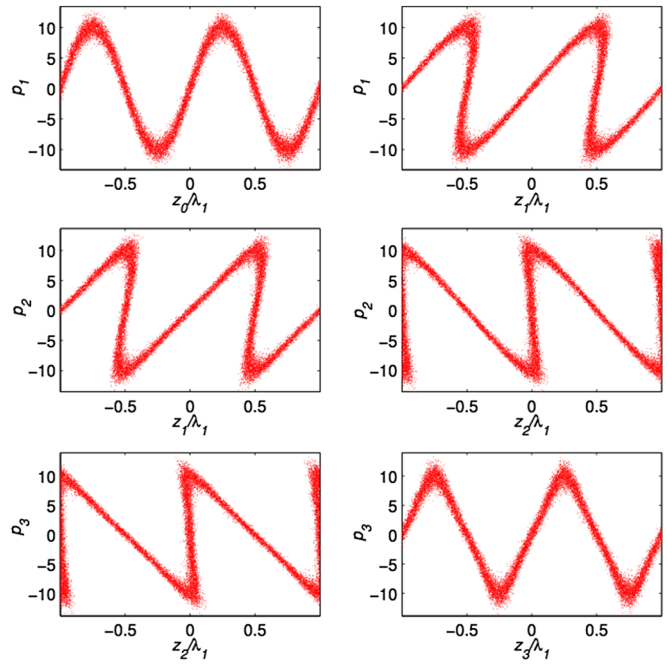

FIG. 4. Synthetic triangle or sawtooth wave generation with three modulations of wavelength λ_1. The initial modulation (top left) is weakly dispersed in the first chicane (top right). Compensation of the curvature takes place in the second modulator (middle left). Reversing the dispersion (middle right) then enables correction of the remaining portion in the third modulator (bottom left). The last dispersion section sets the final waveform shape (bottom right). Here $A_1 = 10, A_2 = A_1/16, A_3 = A_2, B_1 = \pi/2A_1, B_2 = -2B_1, B_3 = -B_2/2, \phi_2 = \pi$, and $\phi_3 = \pi$.

$\phi_2 = \pi$ prevents excitation of even powers of the curvature. Note that the cubic term can be fully compensated with $A_2 = A_1/(1 + A_1B_1)^4 = A_1/16$. However, while this value results in local linearity to fifth order, canceling the cubic term by itself is not sufficient to properly correct for the higher-order curvature near the peaks that originates from the initial sinusoidal modulation. Thus, since the primary function of this arrangement is to synthesize a triangular waveform, optimization necessitates increasing either B_1 or A_2 to slightly overcompensate and reduce the linear slope. This comes at the expense of canceling the cubic term, but leads to macrolinear regions that both closely model the ideal waveforms and contain a larger fraction of particles after dispersion.

A sawtooth wave can be synthesized in a similar fashion, again with a single wavelength. Unlike previously where the second modulation is used to compensate for curvature, here the second modulation acts to effectively remove the chirp at $z_1 = \pm\lambda_1/2$, producing a waveform similar to that of a sawtooth generated by the first two harmonics in Fig. 2. The phase-space evolution is shown in Fig. 5. The final distribution (bottom right) closely approximates an ideal sawtooth shape, and analysis shows that the maximum fundamental bunching factor is about 80%, matching that of the sawtooth generated with three harmonic modulations

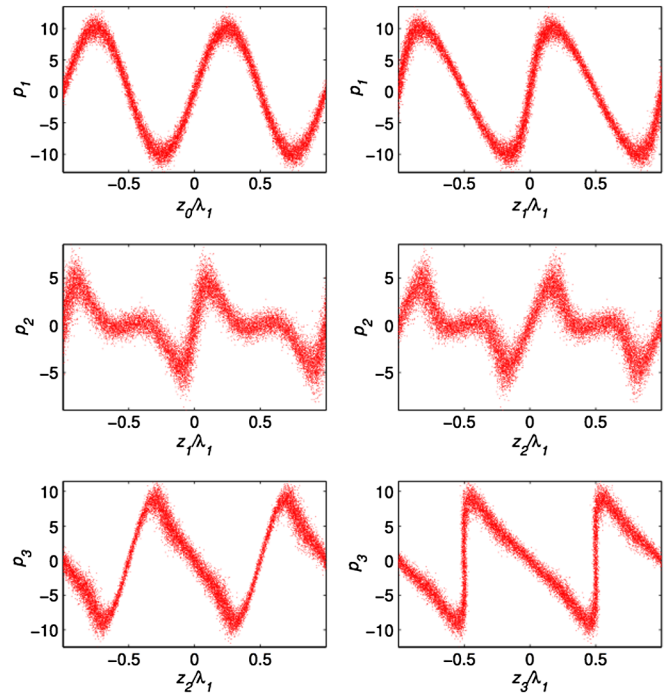

FIG. 5. Synthetic sawtooth wave generation with three modulations of wavelength λ_1. Here $A_1 = 10, A_2 = 3A_1/4, A_3 = A_1, B_1 = -1/2A_1, B_2 = -2B_1, B_3 = 2B_1, \phi_2 = \phi_3 = \pi$.

in Fig. 2. The direction of the sawtooth is reversed by changing the sign of the dispersion in each stage.

Finally, a more complex single-frequency manipulation also generates a synthetic square wave distribution (Fig. 6).

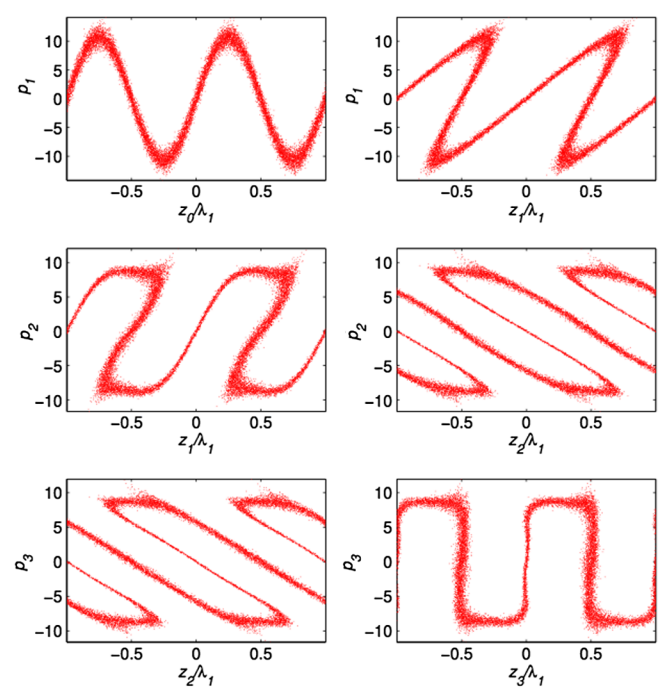

FIG. 6. Synthetic square wave generation with three modulations of wavelength λ_1. Here $A_1 = 10, A_2 = A_1/4, A_3 = A_2/16, B_1 = \sqrt{3}\pi/2A_1, B_2 = -3B_1, B_3 = -3B_2/4, \phi_2 = 0$, and $\phi_3 = \pi$.

This process involves overdispersing the beam in the first chicane to generate a nonlinear phase space. While more complicated, the procedure can be seen to be of the same sort as the triangular wave synthesizer. Namely, reversing the dispersion between modulator sections allows the laser to operate on both the positive and negative regions of local chirp generated by the initial laser; in this case simultaneously. The result is a square waveform of amplitude $\simeq A_1$ and periodicity λ_1. It is interesting to note that the synthetic square wave has density peaks every half period, which leads to partial suppression of the fundamental and all odd-bunching harmonics.

In all three waveform synthesizers, the modulation and dispersion values scale directly with the amplitude A_1 of the initial modulation. Note that, in contrast to the triangle and sawtooth synthesizers, the square wave synthesizer closely resembles the overall shape of the ideal square wave but is quantitatively different from that of modulation from multiple laser harmonics shown in Fig. 2. By inspection one can see that, while the local regions of the distribution become partially linearized, this procedure does not separate the beam into distinct, narrow energy bands.

IV. RADIATION WAVEFORM SYNTHESIZER

While single-frequency modulations mediated by dispersion can synthesize simple waveform distributions in the longitudinal phase space, here we show that the same arrangement can also be used to generate triangular and square *density* modulations in the beam. Because the coherent fields emitted by the beam are a replica of the longitudinal density profile, this allows the possibility of generating square and triangular shaped fields at the scale of the optical wavelength. This is enabled by the freedom one has to control the phase and amplitude of the harmonic bunching components by adjustment of the dispersion and modulation amplitudes. Optical-scale waveforms of this sort are a topic of recent interest [32], and may be ideally suited for resolving atomic-scale processes at the subfemtosecond time scales [22], or in control of quantum systems by matching excitations with properly tuned spectral components [23].

The coherent electric field spectrum produced by a beam is proportional to the beam form factor, given by the Fourier transform of the beam distribution. Assuming a simple model where the emission is dominated by the longitudinal distribution of a highly relativistic beam, the electric field spectrum is

$$E(k) = E_e(k) \int f_f(p, z) e^{-ikz} dp dz, \tag{12}$$

where $E_e(k)$ is the single particle emission kernel. If the radiator bandwidth evenly extends over the spectral domain of harmonics excited in the beam, $E_e(k)$ can be treated as constant. This suggests the use of, for example, coherent transition radiation or coherent edge radiation from a bend magnet. The electric field spectrum is then given by the longitudinal form factor, which is simply the bunching factor $b(k)$ over all frequencies by Eq. (2). By the properties of the Fourier transform, the spatial electric field distribution is thus simply the beam density distribution. As a result, if the complex-valued bunching factor spectrum has the amplitude and phase content as defined in Eqs. (9) and (10), the density distribution will be that of the desired waveform.

Figures 7 and 8 illustrate the final output of different optimizations to produce triangular and square density distributions at the laser wavelength. The longitudinal phase space is shown in red, and the density distribution (found by integration over the energy) is shown in blue. The modulus of the bunching factor spectrum is also shown, and displays a series of harmonic peaks whose magnitudes decrease in accord with the decreasing amplitudes of the waveform harmonics. The triangular density shape in Fig. 7 is produced by adjusting the modulating amplitudes and dispersions to suppress the even harmonics and to excite odd-harmonic amplitudes that decrease quadratically as $1/(2h-1)^2$, each with alternating phase. Similarly, the square-shaped density profile in Fig. 8 is composed of only odd-bunching harmonics in phase, with amplitudes that fall off as $1/(2h-1)$. It is also possible to generate symmetric cosine-series density distributions using all harmonics in phase, with amplitudes scaling as $1/h$. (These have the same Fourier expansion as sawtooth

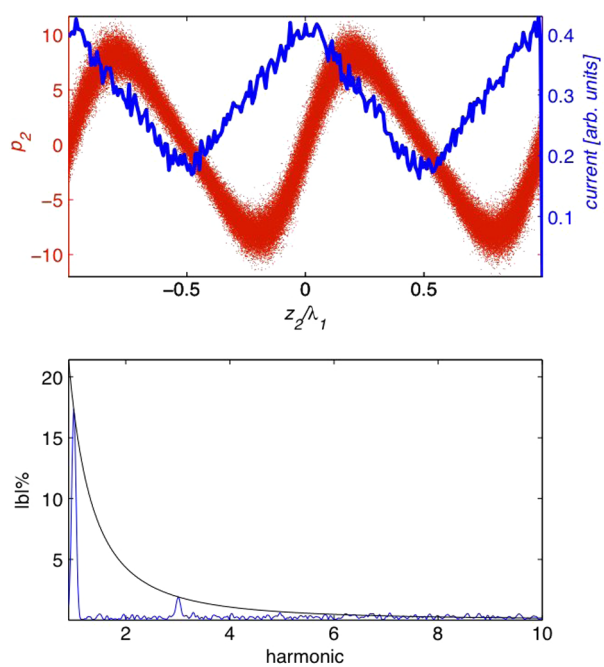

FIG. 7. Three modulator generation of odd-harmonic bunching that goes like $b[(2h-1)k_1] = b(k_1)/(2h-1)^2$ for the emission of triangular radiation fields. Top: Modified phase space and current distribution with $A_1 = 10$, $A_2 = 1.934$, $A_3 = 0.287$, $B_1 = 0.013$, $B_2 = -0.294$, $B_3 = -0.233$, $\phi_2 = \phi_3 = \pi$. Bottom: Bunching factors compared with $1/(2h-1)^2$ dependence of sawtooth amplitudes.

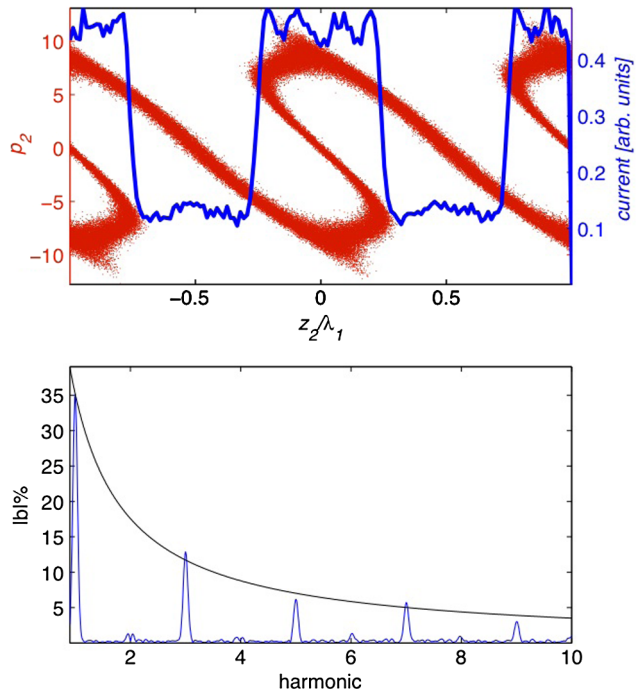

FIG. 8. Two-modulator generation of odd-harmonic bunching with amplitudes $b[(2h-1)k_1] = b(k_1)/(2h-1)$ for the emission of square-wave fields. Top: Modified phase space and current distribution with $A_1 = 10$, $A_2 = 1.388$, $B_1 = 0.295$, $B_2 = -0.551$, $\phi_2 = \phi_3 = 0$. Bottom: Bunching factors compared with $1/(2h-1)$ dependence of square-wave amplitudes.

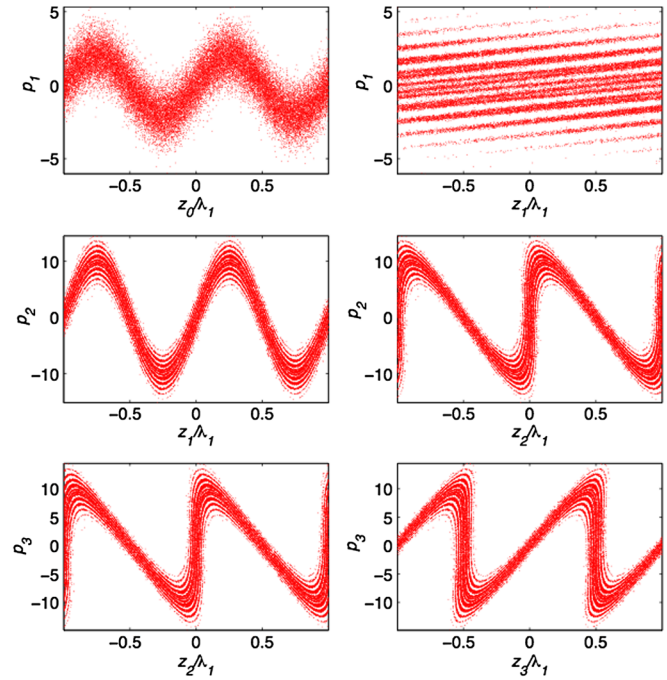

FIG. 9. i-EEHG compensation in third modulator.

waves, but with the sine replaced by cosine.) Finding the proper modulation and dispersion values is just a matter of numerically finding the values of A_1, A_2, A_3, B_1, and so on, such that the bunching factor in Eq. (5) at a given harmonic has the proper amplitude and phase with respect to the first harmonic. Note that the square wave shown in Fig. 8 is formed reasonably well with a simpler two-modulator setup (M-C-M-C). From Eq. (12) the instantaneous field amplitudes $|E(z)|$ calculated from the Fourier transform of the complex bunching factor $\int b(k)e^{ikz}dz$ match the shape of their respective density modulations in blue, demonstrating that the waveforms are generated at scale of the laser wavelength. Note that, within the limits of this framework, asymmetric density distributions like a sawtooth cannot be generated in this fashion because of the symmetric way in which the dispersion transforms the phase space.

V. ENHANCING FEL AND IFEL PERFORMANCE

A. Improved EEHG (i-EEHG)

In standard EEHG, two modulator/chicane modules (M-C-M-C) are used to generate high harmonics in the e-beam bunching with a small associated increase in the total energy spread [8,9,11]. For convenience, here we denote the amplitudes and dispersion strengths of standard EEHG with the superscript 0 to distinguish them from those of the present triple modulator/chicane. EEHG uses a strong chicane in the first stage (B_1^0) to turn the initial sinusoidal modulation with amplitude (A_1^0) into striated energy bands in the phase space. These are then converted into harmonic density peaks after the second modulation (A_2^0) and dispersion (B_2^0) stage. The cubic curvature of the sinusoidal energy distribution is ultimately what leads to the $a^{-1/3}$ scaling of the bunching factor [33]. Thus, linearization of the phase space can ultimately improve the scaling in EEHG, as described in [29,30].

With the addition of a third modulator-chicane section, we find that the partial-linearization procedure performed with a single wavelength can also result in improved bunching factors in EEHG. We refer to this procedure as i-EEHG, and the concept is illustrated in Fig. 9. The approach follows a similar piecewise phase-space manipulation as depicted in Fig. 3, but here linearization takes place in the third modulator only after the beam has undergone the first two stages of EEHG manipulation. This way, the first two-thirds of the setup is essentially standard EEHG with $A_1 = A_1^0$ and $A_2 = A_2^0$, but now the third laser modulator with $A_3 = A_2/16$ is used to linearize the individual energy bands in the decompressed portion of the beam after the second chicane, which has strength $B_2 \simeq -1/A_2 \simeq -B_2^0$. Reversing the dispersion in the third stage by $B_3 \simeq -2B_2$ then stands these bands upright. This results in an enhancement of 20%–25% of the high-harmonic bunching compared with EEHG for the same final energy spread (Fig. 10). Inspection shows that this increase is similar to that obtained by synthesizing a sawtooth with a second harmonic laser in a pre-EEHG injector stage, but here uses a single wavelength. Note that the tuning of

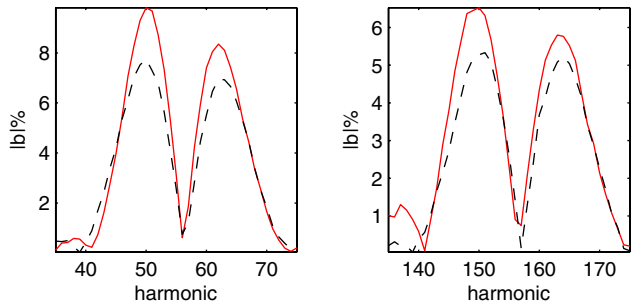

(a) $B_1 = 6.92$, $B_2 = -0.094$, $B_3 = 0.226$ (b) $B_1 = 18.35$, $B_2 = -0.095$, $B_3 = 0.223$

FIG. 10. I-EEHG compensation (red solid line) in third modulator for (a) 50th and (b) 150th harmonic. Standard EEHG is shown as a dashed line. Here $A_1 = A_1^0 = 2$, $A_2 = A_2^0 = 10$, $A_3 = A_2/16$, $\phi_2 = 0$, $\phi_3 = \pi$, $B_2 \simeq -1/A_2$, $B_3 \simeq B_2^0 - B_2$.

i-EEHG is relatively straightforward. For a desired harmonic a, one can optimize the simpler standard two-module EEHG scheme to obtain the necessary dispersions in the first B_1^0 and second B_2^0 sections. These values are then used as offsets for the dispersions in the i-EEHG setup surrounding the compensation section.

It is worth commenting that the final bunching factor in i-EEHG is necessarily sensitive to timing and laser amplitude jitter, particularly in the compensation section. Figure 11 shows a map of the final bunching as a function of A_3 and ϕ_3 for the example parameters given in Fig. 10. Clearly, the tolerances become tighter as the final harmonic number is increased, so the jitter must be controlled at the appropriate level for practical implementation in a given system.

B. Adiabatic buncher

In IFELs, a high-power laser is used to accelerate a charged particle beam inside a magnetic wiggler [15]. The beam is usually injected into the wiggler at near relativistic speeds from a preacceleration stage, and is captured and boosted in energy through the high-gradient laser fields. Because the initial e-beam is evenly distributed across the accelerating phase buckets, the capture efficiency of single-stage IFELs can be rather poor unless the beam is density prebunched at the laser wavelength (multistage). Prebunching by a single modulator/chicane section can increase the overall efficiency to near 80%, but this still leaves a portion of the beam behind during acceleration.

With the triple modulator arrangement, however, it is possible to further increase the bunching factor to boost the capture efficiency. One such possibility (described above) is the generation of a sawtooth-type distribution in the longitudinal phase space with laser harmonics, followed by a dispersive section. With three harmonics, this increases the bunching to about 80% (Fig. 5). One can do even better, however, by utilizing the dispersive sections

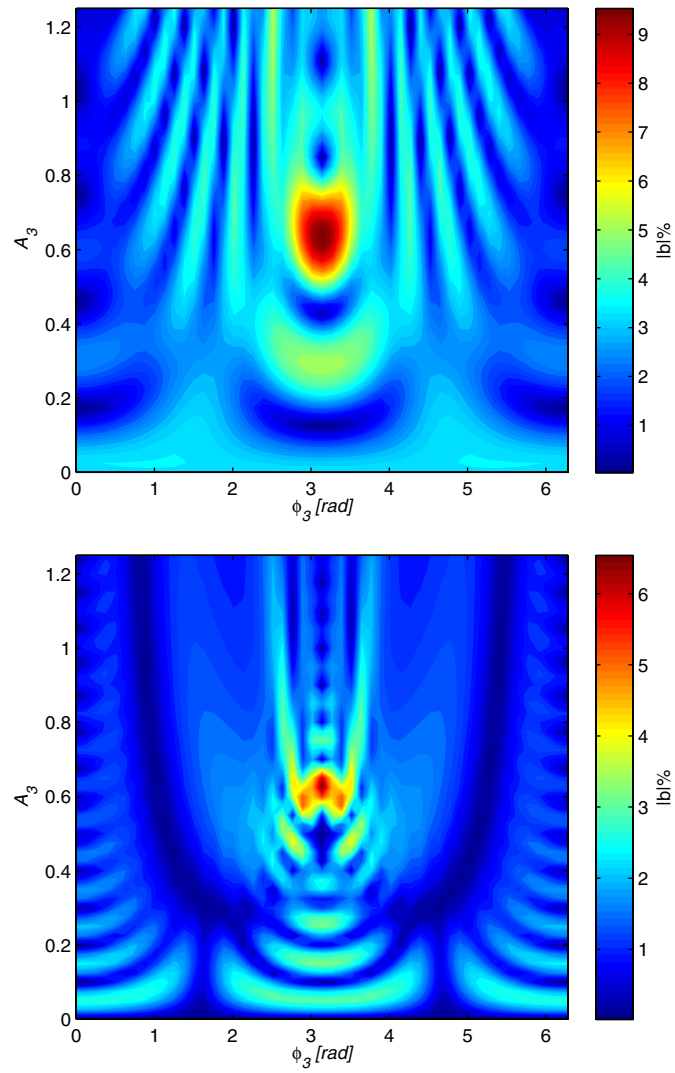

FIG. 11. Bunching factor tolerances of i-EEHG in third modulator for 50th harmonic (top) and 150th harmonic (bottom) using parameters given in Fig. 10.

between modulators and using only a single laser frequency to increase the bunching to over 90%.

In this method, each dispersion section is used to rotate the local phase space so as to deposit the maximum number of particles into the phase region between peaks, $\pi/2 \leq k_1 z \leq 3\pi/4$, after each modulation. The concept is similar to the prebunched enhanced EEHG scheme in [28], but is repeated in each section. The evolution of the phase space is shown in Fig. 12. After an initial modulation of A_1, the first chicane overbunches the beam with $B_1 \simeq 2/A_1$. A second, larger modulation A_2 is again overbunched by the middle chicane with the strength $B_2 \simeq 2/A_2$. By the end of the third chicane, most of the particles have been rolled up into the center of the phase bucket, resulting in a bunching factor of 92% at the frequency k_1. The sharply peaked density distribution is shown in Fig. 13. This beam

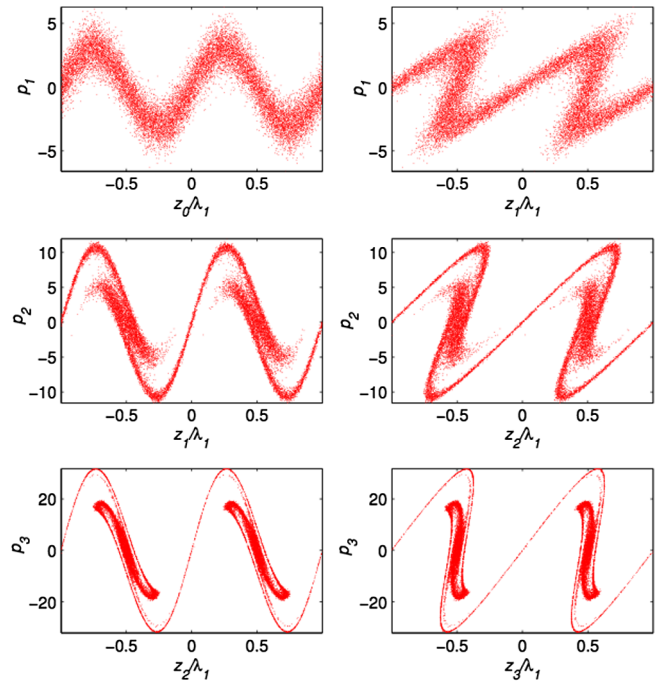

FIG. 12. Adiabatic buncher with three modulations of wavelength λ_1. Here $A_1 = 3$, $A_2 = 3A_1$, $A_3 = 3A_2$, $B_1 = 1.8/A_1$, $B_2 = 2.2/A_2$, $B_3 = 1.55/A_3$, $\phi_2 = \phi_3 = 0$.

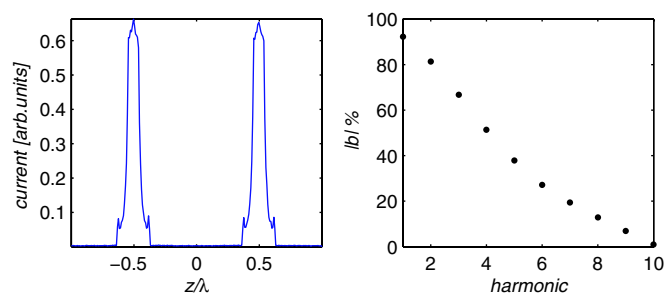

FIG. 13. Current (left) and harmonic bunching factors (right) in the adiabatic bunching scheme.

can then be injected into an optimized IFEL with drive laser frequency k_1 and efficiently accelerated. The use of a single laser wavelength with negligible phase shift between sections to both prebunch and accelerate the beam suggests a simple scenario in which the high-power drive laser performs all the manipulations in sequence. The increasing modulation amplitudes may be optimized, for example, by using an initially large but converging laser spot size such that the modulating field grows in each section and the accelerating stage is positioned at the laser waist. Repeatability in the final bunching depends primarily on timing control between sections. The sensitivity of the system to the arrival phase of the second and third lasers is shown in Fig. 14. Analysis shows that control of each laser phase to within $\pm\pi/2$ is required.

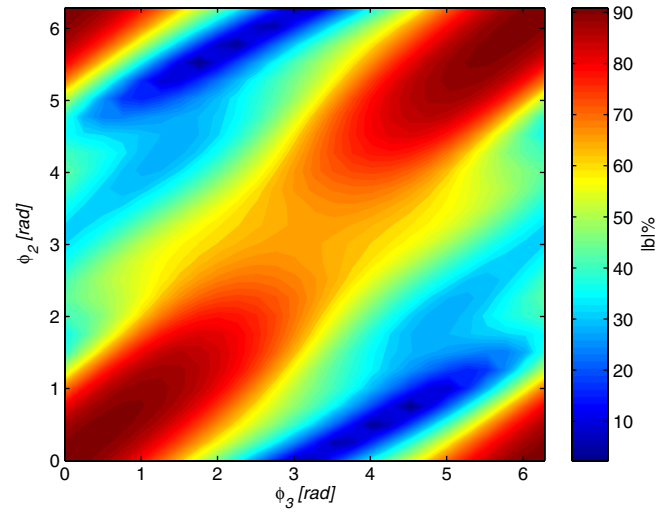

FIG. 14. Tolerance of adiabatic buncher to phase jitter in second and third lasers.

VI. CONCLUSIONS AND DISCUSSION

We have examined the use of a triple modulator/chicane arrangement to perform a variety of optical-scale manipulations on a relativistic electron beam. With only a single laser, this versatile setup can synthesize triangular, sawtooth, and square waveforms in the longitudinal phase space, generate precisely tuned density distributions for the emission of square and triangle waveforms at the optical scale, provide moderate increase in EEHG high-harmonic bunching, and generate bunching above 90% at the laser fundamental frequency to enhance the efficiency of IFEL accelerators.

In our paper we limited our analysis to cases to $N \leq 3$, where N is the number of M-C modules. However, it is straightforward to extend the analysis to $N > 3$ which will provide more accuracy to the surgery of beam longitudinal phase space, at the expense of more complexity in practical implementation. For instance, analysis shows the trap efficiency is approximately $1 - 0.42^N$ in the adiabatic buncher, which indicates that nearly 99% of the particles can be trapped with five M-C modules. With four M-C modules in the i-EEHG scheme, one can linearize the modulation in both modulators and this will further increase the bunching factor at high harmonics.

Several considerations remain for applying these techniques in practice. For instance, the chicanes convert beam energy jitter into timing jitter which changes the phase of the modulation in subsequent modulators. To accurately control the phase, the beam energy jitter needs to be much smaller than the laser energy modulation. The laser timing between sections must also be adequately controlled according to the demands of the particular scheme and parameter space. It should also be mentioned that, for most of the proposed schemes, the beam has significant bunching at the laser frequency in the second and third

modulators. This means the beam will radiate coherent radiation as it goes through the modulator. As the zeroth order approximation, this effect is neglected in our analysis, which is justified when the coherent radiation is much weaker than the external laser. However, depending on the beam peak current and external laser power, the self-interaction between the coherent radiation and the electron beam may need to be accounted for in some cases. Nevertheless, the cascaded modulator-chicane modules promise many advanced optical manipulations and may lead to enhancement in FEL and IFEL performance.

ACKNOWLEDGMENTS

The authors would like to thank A. Fry for useful discussions. This work is supported by U.S. DOE under Contract No. DE-AC02-76SF00515.

APPENDIX

The general form of the bunching factor at the frequency k at the end of the last chicane section is given by the Fourier transform of the longitudinal distribution. From Eq. (2) for $N = 3$ sections,

$$b(k) = \left\langle \int e^{-ikz_3} f_f(z_3, p_3) dp_3 \right\rangle. \tag{A1}$$

As in the cited references, the calculation is simplified by transforming back to the initial variables z_0 and p_0, which gives

$$\begin{aligned} b_{n,m,l} = {} & e^{-\xi_{n,m,l}^2/2 + im\phi_2 + il\phi_3} J_n(-A_1 \xi_{n,m,l}) \\ & \times J_m[-A_2(n + mK_2)(B_2 + B_3) \\ & - lA_2K_3B_3] J_l[-(n + mK_2 + lK_3)A_3B_3], \end{aligned} \tag{A2}$$

with

$$\xi_{n,m,l} = n(B_1 + B_2 + B_3) + mK_2(B_2 + B_3) + lK_3B_3. \tag{A3}$$

The total complex-valued bunching factor is given by the sum over n, m, and l in Eq. (4). With identical wavelengths between sections we set $K_2 = K_3 = 1$. The harmonic number is therefore an integer $a = n + m + l$, and we can replace one of the sums in (A2) to obtain Eq. (6),

$$\begin{aligned} b_{n,m} = {} & e^{-\xi_{n,m}^2/2 + im(\phi_2 - \phi_3) + i(a-n)\phi_3} J_n(-A_1 \xi_{n,m}) \\ & \times J_m[-A_2(n + m)B_2 - aA_2B_3] J_{a-n-m}[-aA_3B_3], \end{aligned} \tag{A4}$$

with

$$\xi_{n,m} = n(B_1 + B_2) + mB_2 + aB_3, \tag{A5}$$

as in Eq. (7).

It is useful to compare the general scaling of the triple modulator scheme with that of simple EEHG. For high-harmonic generation with $m, l > 4$, the Bessel functions J_m and J_l reach their maximal values $0.67/m^{1/3}$ and $0.67/l^{1/3}$ when their arguments are equal to $g(m)$ and $g(l)$, respectively, where $g(x) = \pm(x + 0.81x^{1/3})$. The optimal second and third dispersion values are then given by

$$B_2 \approx \frac{A_2 g(l) - A_3 g(m)}{A_2 A_3 (n + mK_2)}, \qquad B_3 \approx -\frac{g(l)}{aA_3}. \tag{A6}$$

At these values $\xi = nB_1 - g(m)/A_2$, which is kept small due to the $e^{-\xi^2/2}$ factor. Thus, the dispersion in the first section scales like

$$B_1 \sim \frac{g(m)}{nA_2}. \tag{A7}$$

Combined with the peak value of 0.58 for the term $e^{-\xi^2/2} J_1(A_1 \xi)$ for $A_1 \gg 1$, the maximum bunching factor obtainable in the triple modulator scheme for a given set of indices $m, l > 4$ is

$$b_{-1,m,l} \approx \frac{0.26}{(ml)^{1/3}}. \tag{A8}$$

From this expression it becomes clear that implementation of the triple modulator/chicane scheme as a simple extension of the EEHG technique for large m and l results in smaller bunching factors, as seen by comparison with the harmonic bunching in EEHG that goes like $\simeq 0.39/a^{1/3}$. Nevertheless, there are specific optimizations, such as described here and in [25–27], where multiple contributions to the bunching from different m and l add to produce an increased total bunching factor in Eq. (4), specifically when one of either m or l is kept small for $a \gg 1$.

[1] P. Emma *et al.*, Nat. Photonics **4**, 641 (2010).
[2] A. H. Zewail, Annu. Rev. Phys. Chem. **57**, 65 (2006).
[3] P. Musumeci, J. Moody, and C. Scoby, Ultramicroscopy **108**, 1450 (2008).
[4] L. H. Yu, Phys. Rev. A **44**, 5178 (1991).
[5] L.-H. Yu, M. Babzien, I. Ben-Zvi, L. F. DiMauro, A. Doyuran, W. Graves, E. Johnson, S. Krinsky, R. Malone, I. Pogorelsky *et al.*, Science **289**, 932 (2000).
[6] L. H. Yu, L. DiMauro, A. Doyuran, W. S. Graves, E. D. Johnson, R. Heese, S. Krinsky, H. Loos, J. B. Murphy, G. Rakowsky *et al.*, Phys. Rev. Lett. **91**, 074801 (2003).
[7] J. Wu and L. H. Yu, Nucl. Instrum. Methods Phys. Res., Sect. A **475**, 104 (2001).
[8] G. Stupakov, Phys. Rev. Lett. **102**, 074801 (2009).
[9] D. Xiang and G. Stupakov, Phys. Rev. ST Accel. Beams **12**, 030702 (2009).
[10] D. Xiang, E. Colby, M. Dunning, S. Gilevich, C. Hast, K. Jobe, D. McCormick, J. Nelson, T. O. Raubenheimer, K. Soong *et al.*, Phys. Rev. Lett. **105**, 114801 (2010).
[11] D. Xiang, E. Colby, M. Dunning, S. Gilevich, C. Hast, K. Jobe, D. McCormick, J. Nelson, T. O. Raubenheimer, K. Soong *et al.*, Phys. Rev. Lett. **108**, 024802 (2012).

[12] A. A. Zholents, Phys. Rev. ST Accel. Beams **8**, 040701 (2005).
[13] D. Xiang, Y. Ding, T. Raubenheimer, and J. Wu, Phys. Rev. ST Accel. Beams **15**, 050707 (2012).
[14] E. Kur, D. J. Dunning, B. W. J. McNeil, J. Wurtele, and A. A. Zholents, New J. Phys. **13**, 063012 (2011).
[15] R. B. Palmer, J. Appl. Phys. **43**, 3014 (1972).
[16] P. Musumeci, C. Pellegrini, and J. B. Rosenzweig, Phys. Rev. E **72**, 016501 (2005).
[17] W. D. Kimura, M. Babzien, I. Ben-Zvi, L. P. Campbell, D. B. Cline, C. E. Dilley, J. C. Gallardo, S. C. Gottschalk, K. P. Kusche, R. H. Pantell *et al.*, Phys. Rev. Lett. **92**, 054801 (2004).
[18] G. Andonian, E. Hemsing, D. Xiang, P. Musumeci, A. Murokh, S. Tochitsky, and J. B. Rosenzweig, Phys. Rev. ST Accel. Beams **14**, 072802 (2011).
[19] E. Hemsing, P. Musumeci, S. Reiche, R. Tikhoplav, A. Marinelli, J. B. Rosenzweig, and A. Gover, Phys. Rev. Lett. **102**, 174801 (2009).
[20] E. Hemsing, A. Marinelli, and J. B. Rosenzweig, Phys. Rev. Lett. **106**, 164803 (2011).
[21] E. Hemsing and A. Marinelli, Phys. Rev. Lett. **109**, 224801 (2012).
[22] E. Goulielmakis, V. S. Yakovlev, A. L. Cavalieri, M. Uiberacker, V. Pervak, A. Apolonski, R. Kienberger, U. Kleineberg, and F. Krausz, Science **317**, 769 (2007).
[23] R. S. Judson and H. Rabitz, Phys. Rev. Lett. **68**, 1500 (1992).
[24] J. P. Duris, P. Musumeci, and R. K. Li, Phys. Rev. ST Accel. Beams **15**, 061301 (2012).
[25] D. Xiang and G. Stupakov, New J. Phys. **13**, 093028 (2011).
[26] D. Xiang, Z. Huang, and G. Stupakov, Phys. Rev. ST Accel. Beams **12**, 060701 (2009).
[27] C. Feng, J. Chen, and Z. Zhao, Phys. Rev. ST Accel. Beams **15**, 080703 (2012).
[28] C. Feng, D. Wang, and Z. Zhao, in Proceedings of FEL 2010, Malmö, Sweden (2010), pp. 629–631.
[29] G. Stupakov and M. Zolotorev, in Proceedings of FEL 2011, Shanghai, China (2011), pp. 45–48.
[30] D. Ratner and A. Chao, in Proceedings of FEL 2011 Conference, Shanghai, China (2011), pp. 53–56.
[31] A. Marinelli, J. B. Rozenzweig, and E. Hemsing, Phys. Rev. Lett. (to be published).
[32] H.-S. Chan, Z.-M. Hsieh, W.-H. Liang, A. H. Kung, C.- K. Lee, C.-J. Lai, R.-P. Pan, and L.-H. Peng, Science **331**, 1165 (2011).
[33] G. Stupakov (private communication).